Applied Geochemistry 135 (2021) 105119

Contents lists available at ScienceDirect

Applied Geochemistry

journal homepage: www.elsevier.com/locate/apgeochem

Geochemical characterization of dust from arsenic-bearing tailings, Giant Mine, Canada

Alexandra S. Bailey *, Heather E. Jamieson, Anežka Borčinová Radková

Department of Geological Sciences and Geological Engineering, Queen's University, Miller Hall, 36 Union Street, Kingston, ON, K7L 3N6, Canada

ARTICLE INFO

Editorial handling by Dr. Z Zimeng Wang

Keywords:
Arsenic
Arsenic speciation
Tailings
Dust
Maghemite
Mimetite
Calcium-iron arsenate

ABSTRACT

Dust from uncovered mine tailings at Giant mine, an abandoned mine in northern Canada, has been a concern for nearby residents. We have utilized microanalytical mineralogical analysis combined with quantitative measurements of phase distribution and bulk concentration to fully characterize the dust currently generated from the Giant mine tailings. Surface tailings material was sampled from three tailings impoundments on site and sieved to <63 μm as a proxy for dust, and total suspended particulate (TSP) samples were collected continuously over two months to represent the airborne material that is generated from the tailings. Inductively coupled plasma-optical emission spectrometry (ICP-OES) and -mass spectrometry (ICP-MS) show elevated concentrations of As, Sb, Zn, Pb, Cu and Ni in all samples; comparison of results for sieved and unsieved samples show that As is more concentrated in the <63 μm fraction of the tailings. The X-ray absorption near edge structure (XANES) results for the tailings indicate that the As in the samples is a mixture of As^{1-}, As^{5+} and As^{3+}. Scanning electron microscope-based mineral liberation analysis (SEM-MLA) results show that roaster-generated iron-oxides (i.e., maghemite), calcium-iron arsenate (i.e., yukonite), and arsenopyrite comprise the majority of the As-bearing particles in the surface tailings; of these three solid phases, calcium-iron arsenate poses the greatest risk to human health as it exhibits the highest relative bioaccessibility. A rare lead arsenate phase, which may be bioaccessible, was also detected in minor quantities in the surface tailings; this phase was identified as mimetite through μXRD analysis. Very little arsenic trioxide was found in the surface tailings samples, and no arsenic trioxide was found in the TSP samples; this is because the tailings that were exposed to arsenic trioxide-bearing roaster stack emissions during the 1950s and 1960s have been buried by more recent tailings. Soils near the Giant mine tailings have been found to contain arsenic trioxide from historic stack emissions, which indicates that the mine-impacted environmental media surrounding a tailings impoundment could in some cases pose a greater risk to environmental and human health than the tailings themselves.

1. Introduction

Windblown and vehicle-raised dust from uncovered mine tailings pose a risk to the environment and to local communities through the transport of fine-grained material which may contain high concentrations of metals and metalloids of environmental concern. Climate change is expected to include drought conditions that would exacerbate this process across mining regions (Clemente and Huntsman, 2019). Exposure to mineral dusts (i.e., tailings dust), particularly metal (loid)-bearing mineral dusts, can be detrimental to human health; this is documented in epidemiological studies of atmospheric pollutants (Hamilton, 2000; Engelbrecht and Derbyshire, 2010; Wiseman, 2015; Mwaanga et al., 2019; Tian et al., 2019). Furthermore, tailings dust can have lasting impacts on environmental media such as soils and surface water (Kříbek et al., 2014; Cleaver et al., 2021; Sracek et al., 2021).

The ease at which tailings dust can be suspended by wind, transported, and solubilized in environmental media and human gastro-intestinal and respiratory fluids (i.e., bioaccessibility) is largely dictated by the particle size and mineralogical composition of the dust (Plumlee and Morman, 2011; Martin et al., 2016; Kastury et al., 2019). Fine dust (i.e., less than 10 μm diameter) is able to be suspended for upwards of 300 km (Livingstone and Warran, 1996). It can travel deep in the gastro-intestinal and respiratory systems (Kastury et al., 2019), and it is more reactive than coarse dust (i.e., 50 μm–100 μm diameter) due to the higher relative surface area of the particles (Lippman et al., 1980; Plumlee et al., 2006; Martin et al., 2014). The mineralogical

* Corresponding author.
E-mail address: asbailey517@gmail.com (A.S. Bailey).

https://doi.org/10.1016/j.apgeochem.2021.105119
Received 19 July 2021; Received in revised form 19 October 2021; Accepted 22 October 2021
Available online 23 October 2021
0883-2927/

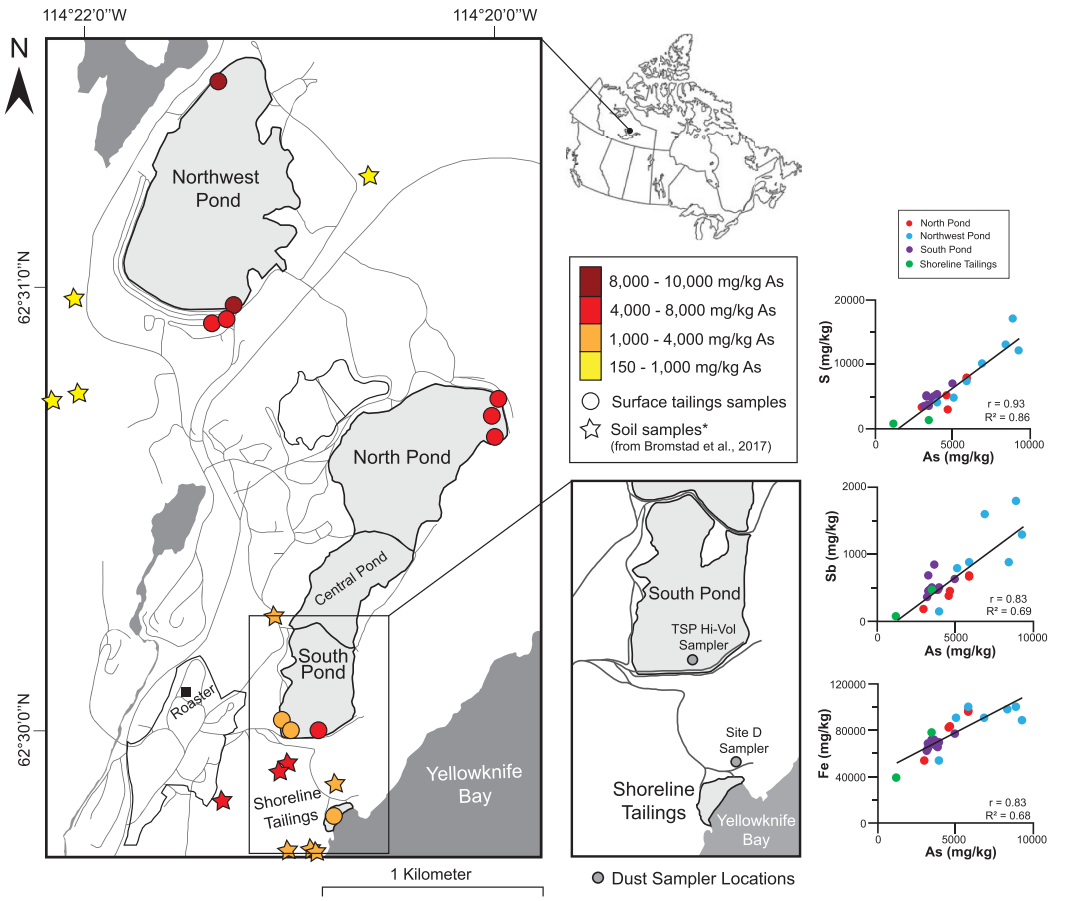

Fig. 1. Map of tailing samples locations (left) and dust sampler location (right). As concentrations from near-surface tailings samples collected for this study are indicated by circles; soil samples from Bromstad et al. (2017), indicated by stars, have been included for comparison. Regression analyses are also included for select elements compared to arsenic in the tailings.

Table 1
Concentrations of constituents of concern (As, Sb, Cu, Pb, Ni, Zn) in sieved and unsieved tailings from North pond, Northwest pond, and South pond compared with soils in the area (Bromstad et al., 2017; Jamieson et al., 2017) and soil quality guidelines set by the Canadian Council of Ministers of the Environment (CCME, 2021). All concentrations in mg/kg; *n* refers to sample count.

	CCME Soil Quality Guideline by Land-Use Category (mg/kg)		Concentration of Metal(loid) in Giant Mine Tailings (mg/kg) $n = 7$ (unsieved), 17 (sieved)		Soil on Giant Mine Property $n = 63$	Regional Soils within 30 km of Giant Mine $n = 479$
	Residential	Industrial	Unsieved	Sieved (<63 μm)	Unsieved	Unsieved
Arsenic (As)	12	12	3000–4000	3200–9300	24–7678	<1 - 4700
Antimony (Sb)	20	40	160–690	370–1800	0.02–352	<1 - 160
Copper (Cu)	63	91	40–82	62–150	5–359	–
Lead (Pb)	140	600	110–250	130–650	1–229	<10 - 220
Nickel (Ni)	45	89	59–78	68–140	2–107	–
Zinc (Zn)	250	410	140–300	160–620	2–453	–

composition of the dust greatly influences the solubility of the particles in bodily fluids, which range from acidic in the gastric system to circum-neutral in the respiratory system (Plumlee et al., 2006). Mineralogical characterization of tailings dust, therefore, is important in determining the risk that the material poses to environmental media and human health.

Although there is a general understanding of the risks posed by tailings dust, there are still major gaps in the literature concerning the chemical form or speciation of dust. Studies investigating the composition of dust sourced from tailings piles have become more common (Martin et al., 2014; Ettler et al., 2019; Ng et al., 2019); however, dust studies pairing chemical speciation work with isolated particle size fractionation remain relatively underrepresented in the literature (Martin et al., 2014; Wiseman, 2015). The studies that have been conducted often lack direct characterization of the amorphous phases present and relative proportions of metal(loid) solid phase hosts. Mineralogical analyses, namely XRD and SEM, have been increasingly utilized in combination with bulk chemical analyses for more detailed characterizations of tailings-sourced dust (Querol et al., 2000; Moreno et al., 2007; Engelbrecht et al., 2009). The limiting factor in these mineralogical analyses is often sample concentration, as it can be difficult to acquire enough airborne dust for XRD analysis. Synchrotron-based methods, such as XANES, μXRF and μXRD, have been applied to speciation studies of dust, as these methods are non-destructive and can analyze particles at the micron scale (Walker et al., 2011; Corriveau et al., 2011; Kim et al., 2013; McDaniel et al.,

Table 2
Summary of As-hosting solid phases included in the SEM-MLA mineral reference library developed for this study. The average As concentrations, where n refers to the number of analyses, for roaster Fe-oxides (n = 27), Cu–Fe arsenate (n = 8), Pb arsenate (n = 10), Ca–Fe arsenate (n = 12) and Fe oxyhydroxide (n = 16) were calculated from EMPA data collected as part of this study. Mineral phase densities from Webmineral (2017).

Solid Phase	Chemical Formula	Definition	Average As Concentration (wt%)	Phase Density (g/cm^3)
Roaster Fe-Oxide	$Fe^{3+}{}_2O_3(As_{0.066})$	Roaster-generated Fe-oxide; maghemite model compound	3.00	4.90
Cu–Fe Arsenate	$Fe^{3+}{}_{1.92}Cu_{0.71}(As_{0.71}O_4)O$	Cu–Fe–As oxide; phase density from auriacusite	18.6	4.45
Pb Arsenate	$Pb_{2.1}As_{1.4}O_{12}Cl(7H_2O)(Ca_{0.34})$	Pb–As oxide; phase density from mimetite	12.9	7.26
Ca–Fe Arsenate	$Ca_{0.67}Fe^{3+}{}_{3.8}As_{1.2}O_8(OH)_3(5H_2O)(Si_{0.27})$	Ca–Fe arsenate; forms an oxidation rim on arsenopyrite, likely a co-precipitate; phase density from yukonite	14.9	2.65
Fe Oxyhydroxide	$Fe^{3+}O(OH)(As_{0.028})(Ca_{0.045})(Si_{0.068})$	Fe oxyhydroxide forms an oxidation rim on pyrite and pyrrhotite and hosts a small amount of As; a mix of ferrihydrite and goethite, phase density from goethite	2.22	3.80
As-bearing Pyrite	$Fe^{2+}As_{0.02}S_2$	As-bearing sulfide from ore body; arsenian pyrite model compound	1.23	5.01
Arsenopyrite	$Fe^{3+}AsS$	Arsenic sulfide from ore body; arsenopyrite model compound	46.0	6.07
As-Sulfide	As_4S_4	Arsenic sulfide; realgar model compound	70.0	3.56
Arsenolite	As_2O_3	Arsenic trioxide; arsenolite model compound	75.7	1.00

2019; Kastury et al., 2019); however, analysis solely relying on micro-analytical methods can limit representability of data. In this study, we have combined detailed microanalytical work with quantitative measurements of phase distribution and bulk concentration to fully characterize a specific dust source.

The objective of this research, which was carried out as part of a Master's thesis (Bailey, 2017), was to identify arsenic-hosting solid phases in the fine fraction of near-surface tailings and tailings dust from the Giant gold mine. The mine is located just north of City of Yellowknife and is currently undergoing remediation by the Canadian federal government. At the time of writing, the tailings remain uncovered and concern has been expressed by the residents of NDilo, a Yellowknives Dene First Nation community located 2.5 km south-southeast of the tailings area, regarding dust that occasionally reached the community in the late spring after snowmelt and before the tailings were dry enough for dust suppressant to be applied. At that time of year, the exposed tailings are vulnerable to high velocity winds from the north.

2. Background

The geology, ore mineralogy and ore processing history of the Giant mine has been described by Walker et al. (2015). It was a large and long-lived mine and produced 7 Moz of gold from 1949 to 2004 from a mostly underground operation. There are 16 million tonnes of tailings covering 95 ha in several areas which are referred to as ponds although there is only intermittent surface water present. The gold is hosted in arsenopyrite and because of its refractory nature, roasting was used as a pre-treatment for cyanidation. This resulted in three solid waste streams: flotation tailings, cyanided calcine residue and cyanided electrostatic precipitator (ESP) dust which, during most of the operation's history, were combined and sent to the tailings ponds. The tailings do not produce acidic drainage due to the relatively low concentration of sulfide minerals, the removal and oxidation of some of the arsenopyrite in the roaster, and the presence of dolomite and calcite (Walker et al., 2015). In the flotation tailings 70–80% of the particles are <75 μm in diameter; in the calcine 90% of the particles are <45 μm in diameter; and in the ESP residue 90% of the particles are <14 μm in diameter (Walker et al., 2015). The arsenic-hosting solid phases in these three waste streams has been described previously (Walker et al., 2005, 2015; Fawcett and Jamieson, 2011), particularly the roaster-generated iron oxides (i.e., maghemite and hematite) that include up to several weight percent arsenic.

Arsenic trioxide, which is considered the most toxic, bioaccessible and soluble arsenic compound (Jamieson, 2014; Plumlee and Morman, 2011), was also produced in the Giant mine roaster. In the first few years of mine operations (1949–1951), the lack of emission controls on roaster stack emissions resulted in the direct release of arsenic trioxide to the atmosphere. In total, 20,000 tons of arsenic trioxide were released through stack emissions, and 86% of it was released before 1963 (Wrye, 2008). Particles of arsenic trioxide have been observed in near-surface soils on the mine property (Bromstad et al., 2017) and in both soils and lake sediments within 30 km of the former roaster (Jamieson et al., 2017; Van Den Berghe et al., 2018; Schuh et al., 2018: Palmer et al., 2021). Over the life of the mine, most of the arsenic trioxide (237,000 tons) was captured and stored underground.

Prior to this study, there was little information available regarding the composition of the dust-sized fraction of the surface tailings at Giant mine. This study determines which arsenic-hosting solid phases predominate the dust-sized fraction of the tailings, and whether arsenic trioxide is among them.

3. Methods

3.1. Sample collection

The two types of dust samples characterized in this study were near-

surface tailings sieved to <63 μm as a proxy for dust and dust collected in a high-volume total suspended particulate (TSP) sampler. Eighteen tailings samples were collected in October 2015 from the top 10 cm (cm) of the three main tailings ponds on the Giant mine site (i.e., North Pond, Northwest Pond, and South Pond) and from the shoreline tailings site (Fig. 1), which represents the oldest tailings at Giant mine. The surface tailings samples were dry at the time of collection, and were stored at room temperature and exposed to oxidizing surface conditions during sample preparation and analysis. Twenty-two sub-samples were collected from the bulk tailings samples using multiple riffle-type sample splitters to create homogeneous and representative sub-samples; nineteen of these sub-samples were sieved to <63 μm and three were unsieved. Polished thin sections of these samples were made with minimal use of water to preserve soluble phases.

The high-volume TSP dust sampler (TE-5005 model) was positioned directly on the tailings at the south end of South Pond (Fig. 1) and was continuously sampled over a period of two months, from May 16 to July 18, 2016. Pre-weighted 20 cm by 25 cm quartz fiber filters were used as media to collect suspended particles <100 μm in diameter. A sampling interval of two to three days was found to produce sufficient TSP for mineralogical analyses without causing the filter to disintegrate. At the end of the sampling period, filters were removed from the filter holder, promptly folded in half with the dust-bearing side facing inwards, placed in a folder, and sealed in an envelope. Sub-samples for ICP-MS analysis were cut into 10 cm by 25 cm pieces, and sub-samples for SEM analysis were cut into 2.5 cm^2 pieces. Filters were cut using stainless steel scissors which were cleaned with ethanol between uses.

3.2. Multi-element analysis

Twenty-one surface tailings sub-samples were sent to Queen's University Analytical Services Unit (ASU) for multi-element bulk chemical analysis using inductively coupled plasma mass spectrometry (ICP-MS) and inductively coupled plasma optical emission spectrometry (ICP-OES). Samples were digested using aqua regia at 90 °C (°C). The Agilent 7700x model was used for the ICP-MS analyses, and the Agilent VistaPRO CCD was used for the ICP-OES analyses. Three sets of duplicates were prepared and analyzed at ASU, along with a certified reference material and one blank per sample sub-set.

Twenty-three TSP quartz fiber filters were analyzed at Maxxam Analytics for multi-element bulk chemical analysis via ICP-MS. Filters were digested using aqua regia and were analyzed following the USEPA 6020A reference method. One processed blank and two spike blanks (i.e., quartz fiber filter strips spiked with a known amount of lead and carried through extraction process) were included by Maxxam for quality control. Calibration for ICP-MS analysis was done with a calibration blank and five calibration standards. A continuing calibration blank (CCB), continuing calibration verification (CCV), and low level CCV (same source as calibration) were analyzed after every ten samples and at the end of the analytical run.

3.3. Scanning electron microscopy (SEM)

The 22 surface tailings sub-samples were analyzed using scanning electron microscopy (SEM) coupled with automated mineralogy to determine the concentration of arsenic-bearing mineral phases and the percent arsenic distribution in each sample. Thin sections were carbon-coated prior to analysis. The automated mineralogy software, Mineral Liberation Analysis (MLA), was used to collect chemical data for each particle detected in the sample via energy-dispersive X-ray spectroscopy (EDS) with the Quanta Field Emission Gun (FEG) and back-scatter electron (BSE) detector. SPL-Lt measurements were collected over a period of 6 h for each sample, and the SEM operated with voltage 25 kV, spot size 5.70–6.00 μm, working distance 10–15 mm, and 500x magnification; samples were standardized to gold. The mineral reference library used to identify solid phases in the samples was compiled as a part of this study to be representative of the Giant mine tailings mineralogy. The mineral reference library was finalized based on observations of grain morphology, grain-by-grain SEM-EDS analysis, grain-by-grain electron microprobe analysis (EMPA), and EMPA molar ratio plots.

Twenty-seven sub-samples of TSP quartz fiber filters were analyzed through SEM-based point counting; quality of data was ensured by analyzing two replicate samples and one blank. Each filter was carbon-coated, and the MLA software was used to collect 250 SEM-BSE frames at 300x magnification and stitch the images together, resulting in a full SEM-BSE image of the sample. During image acquisition, the SEM operated with voltage 25 kV, spot size 4 μm, and working distance 10–15 mm; samples were standardized to copper. Chemical data for select particles was collected via EDS with a Quanta FEG and BSE detector. Sample images were uploaded to Adobe Photoshop®, and metal (loid)-bearing particles were isolated for particle point counting based on their gray scale values. Metal(loid)-bearing particles were defined as those with a gray scale value greater than 90, based on EDS chemical data collected for particles and observations of grain morphology. Particles with gray scale values greater than 90 were selected and exported to ImageJ for point counting.

3.4. Electron microprobe analysis (EMPA)

EMPA of secondary minerals was conducted on three carbon-coated thin sections. Analyses were done using a JEOL JXA-8230 electron microprobe in wavelength-dispersive mode (WDS) with an accelerating voltage of 15 kV, a beam current of 10 nA, a focused beam, and a Pouchou and Pichoir XPP matrix correction (Pouchou and Pichoir, 1988). Calibration was conducted using the following standards: As_2O_5 (synthetic loellingite), Fe_2O_3 (hematite), Cu_2O (cuprite), MnO (synthetic hausmannite), CaO and SiO_2 (wollastonite), SO_3 (barite), PbO (alamosite), and Sb_2O_5 (stibnite). The following lines and detector crystals were used for each peak during calibration: As (Lα, TAP), Fe (Kα, LiFL), Cu (Kα, LiFL), Mn (Kα, LiFL), Ca (Kα, PET), S (Kα, PET), Si (Kα, TAP), Pb (Mα, PETH), Sb (Lα, PETH).

3.5. Synchrotron micro-analysis

Synchrotron-based X-ray absorption fine structure (XAFS) was conducted at Sector 20-BM at the Advanced Photon Sources (APS) at Argonne National Laboratory in Lemont, IL, USA via X-ray absorption near edge structure (XANES) to characterize the solid phase oxidation state of arsenic in 12 tailings sub-samples (both sieved and un-sieved) which were uniformly spread and sealed in Kapton tape. The XANES analyses were performed within a cryostat chamber (12-55 K) to avoid any beam-induced changes to arsenic speciation. The beamline uses a silicon 111 monochromator with rhodium-coated toroidal focusing mirror. Transmission measurements were done with a detector oriented in line with the incident beam, and samples were mounted at 45° relative to the incident beam which was 7 mm wide. A gold energy reference foil was used throughout the experiment, and a platinum foil was used as a reference during calibration for arsenic. The arsenic K-edge referred to in this study is 11867eV; XANES scans spanned from 150eV before the arsenic K-edge (i.e., 11717eV) to approximately 300eV past the arsenic K-edge (i.e., 12167eV). The arsenic edge region was defined as 20eV below the arsenic K-edge to 30eV above the K-edge (i.e., 11,847–11897eV). The mineral standards used for linear combination fit (LCF) references were arsenopyrite (As(-I)S), realgar (As(II)–S), orpiment (As(2.5)-S), hematite (As(III)–O), and maghemite (As(V)–O). XANES data processing was done using the program ATHENA (Demeter 0.9.24).

Synchrotron-based micro X-ray fluorescence (μXRF) and micro X-ray diffraction (μXRD) analyses were conducted at the GSECARS (University of Chicago) beamline 13-IDE at Sector 13 of APS, Argonne National Laboratory (Lemont, IL, USA) for six thin sections. Beamline 13-IDE is a

monochromatic, undulator-based beam which operated with a 2 μm beam diameter at 18.0 KeV for this experiment. The XRF detector used at this beamline is a Vortex ME4 silicon draft diode (SSD) array, and the XRD detectors are a PerkinElmer XRD 1621 amorphous silicon area detector and a MAR CCD area detector. Samples were positioned at 45° relative to the beam. The CCD detector was calibrated prior to analysis using CeO_2 as a standard. Calibrations of and corrections for the μXRD data were done using Dioptas software. The data output from Dioptas was uploaded to HighScore Plus for phase identification.

4. Results

4.1. Near-surface tailings results

4.1.1. Multi-element chemistry

ICP-MS and ICP-OES data show that As, Sb, Cu, Pb, Ni and Zn are all present in relatively high concentrations in the near-surface tailings (Table 1). Several of these constituents (i.e., As, Sb, and Pb) are more highly concentrated in the <63 μm fraction of the tailings; for example, the maximum arsenic concentration measured for the unsieved tailings is 4000 $mgkg^{1-}$, whereas the maximum arsenic concentration in the <63 μm fraction of the tailings is 9300 $mgkg^{1-}$ (Figs. 1 and 2). The highest metal(loid) concentrations were observed in samples from Northwest Pond; North Pond and South Pond exhibit similar ranges of metal(loid) concentrations. In many cases, the concentrations are higher than the guidance criteria for Canadian industrial soils (CCME, 2017). Although mine tailings are not expected to meet these criteria, windblown dust that reaches communities can raise the concentrations in near-surface soils to values approaching the guidelines.

Data for the 22 tailings samples show that arsenic exhibits the best positive correlation with sulfur ($R^2 = 0.86$), followed by antimony ($R^2 = 0.69$) and iron ($R^2 = 0.68$). These data suggest that the arsenic in the near-surface tailings at Giant mine are primarily associated with sulfide minerals, and to a lesser extent iron-bearing phases. The Giant mine ore deposit is characterized by high arsenic and antimony concentrations, which supports the positive correlation observed between arsenic and antimony in the near-surface tailings samples.

4.1.2. SEM and EMPA

Arsenic-hosting phases were identified through SEM analysis, and their chemical composition was then determined through EMPA (Table 2). The iron oxides generated through roasting at Giant mine exhibit distinct physical and chemical properties which make them relatively easy to identify. The roaster iron oxides exhibit a porous, concentric texture and are commonly present as liberated mineral surfaces (Fig. 2); some contain relict arsenopyrite, pyrite, or pyrrhotite at their center (Fig. 2). The roaster iron oxide grains identified in this study exhibit arsenic concentrations between 1.2 wt% and 6.1 wt% (Table 3), which is within the range observed by Walker et al. (2005) (i.e., <0.5 wt % to 7.6 wt%). Iron concentrations in the roaster oxides range from 61 wt% to 69 wt% (Table 3). Based on these data, the roaster iron oxides have been defined as 68% iron, 29% oxygen, and 3% arsenic in the SEM-MLA mineral reference library (Table 2).

SEM-MLA results show that roaster-generated iron oxides are the most abundant arsenic-hosting phase in the Giant mine tailings (Fig. 3). Based on the average arsenic content of the iron oxides, they host approximately 48% (±14%) of the total arsenic in the surface of the tailings ponds (Fig. 3). Arsenopyrite comprises between 2% and 18% of the arsenic-bearing phases in the tailings samples, but accounts for an average of 46% (±16%) of the total arsenic therein (Fig. 3). In all of the near-surface tailings samples, both sieved and un-sieved, these two phases consistently host the greatest proportion of arsenic.

Calcium- and arsenic-bearing oxidation rims were observed on arsenopyrite, pyrite, and pyrrhotite grains in the near-surface tailings samples (Fig. 2). EMPA data show that the oxidation rims on arsenopyrite grains are chemically distinct from the oxidation rims on grains of pyrite and pyrrhotite. Fig. 4 shows EMPA data plotted as As_2O_5 wt% versus Fe_2O_3 wt%. These data show that the iron/arsenic molar ratio for the arsenopyrite oxidation rim falls between 1.4 and 4; while the iron/arsenic molar ratio for the pyrite and pyrrhotite oxidation rims is greater than 9. Based on these data, oxidation of arsenopyrite appears to produce a Ca–As–Fe phase that is trending toward calcium-iron arsenate, while oxidation of pyrite and pyrrhotite trends toward ferrihydrite and goethite (Fig. 4). The molar ratio of calcium/arsenic for the arsenopyrite oxidation rims largely fall at or below 0.67, trending toward yukonite. These results are consistent with those of Walker (2006), who observed similar weathering rims on sulfide grains in the Giant Mine Townsite, located adjacent to Giant mine.

Based on EMPA data collected for the arsenopyrite oxidation rims, they are defined as calcium-iron arsenate with 14.9 wt% arsenic in the SEM-MLA mineral reference library; the pyrite and pyrrhotite rims are defined as iron oxyhydroxide with 2.2 wt% arsenic (Table 2). SEM-MLA results show that calcium-iron arsenate comprises between 12% and 31% of the arsenic-hosting phases in the near-surface tailings and 4.6% (±2.1%) of the total arsenic therein (Fig. 3). Iron oxyhydroxide hosts, on average, 1.4% (±1.8%) of the total arsenic in each sample.

A copper-iron arsenate phase was observed in the tailings samples which is texturally similar to the roaster-derived iron oxides but exhibits higher concentrations of arsenic and copper (Fig. 2, Table 4). This phase contains, on average, 18.6 wt% arsenic, 14.6 wt% copper, and 34.6 wt% iron (Table 4). Fig. 5 shows EMPA data for this phase plotted as Cu_2O wt % versus As_2O_5 wt%. These data show that there is significant compositional variation within individual copper-iron arsenate grains, which suggests that it is actually a mixture of phases. Most of the particles analyzed for this phase exhibit copper/arsenic molar ratios greater than 1.5 or between 1 and 0.5 (Fig. 5). Copper/iron molar ratios are similarly divided, where particles fall either greater than 1 or between 0.5 and 0.125; these data suggest that copper and iron are inversely related in this phase.

A lead- and arsenic-bearing oxide phase (i.e., lead arsenate) was identified in each of the tailings samples. This phase has a distinctly porous texture and is often seen as an oxidation rim on galena (Fig. 2). EMP-WDS spectra show that this phase contains arsenic, lead and chlorine. Fig. 5 shows EMPA data for this phase plotted as As_2O_5 wt% versus PbO wt%. Arsenic/lead molar ratios for this phase range from 0.5 to 0.024, which indicates that there is compositional variation across individual particles of this phase. The bulk of the EMPA data is trending toward mimetite, with one point trending toward sahlinite; mimetite and sahlinite are both lead arsenate minerals that contain chlorine. Based on these data, this phase has been defined as lead arsenate with 12.9 wt% arsenic and 53.1 wt% lead (Table 2).

Out of all 22 near-surface tailings samples processed using SEM-MLA, where an average 287,321 (±121,340) particles were analyzed per sample, only three particles of arsenic trioxide (As_2O_3) were detected in total. Three samples contained one particle each of arsenic trioxide (i.e., ABNWP-1a, ABNWP-3a, ABSP-2a), which were present as liberated particles (Fig. 2).

Antimony is a trace constituent in most of the arsenic-bearing phases

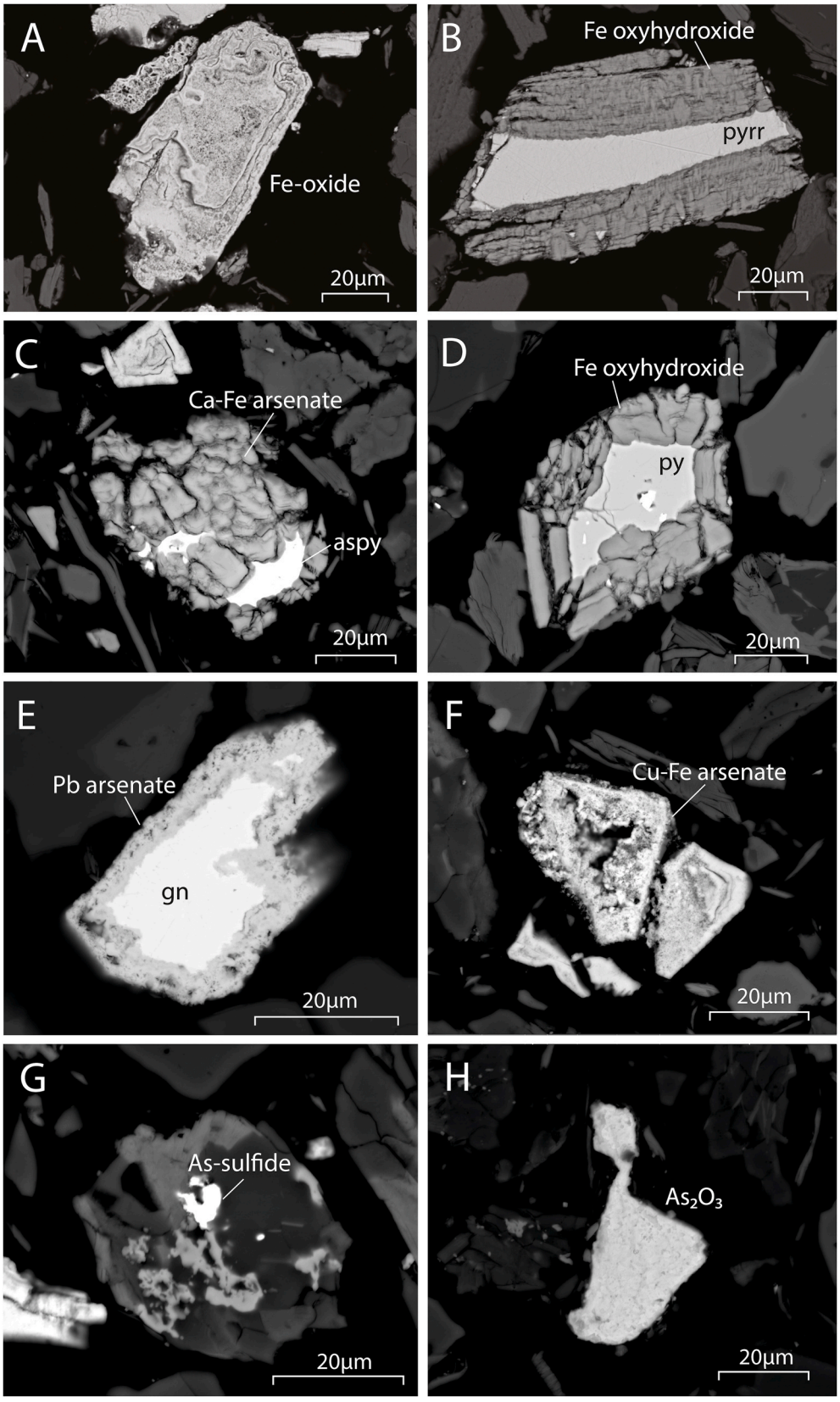

Fig. 2. SEM-BSE images taken of arsenic-hosting phases in the Giant mine tailings. (A) Example of a typical roaster Fe-oxide grain (from sample ABNP-1a); (B) Fe oxyhydroxide weathering rim on pyrrhotite (from sample ABSP-2a); (C) arsenopyrite with Ca–Fe arsenate weathering rim (from sample ABNWP-1a); (D) Fe oxyhydroxide weathering rim on pyrite (from sample ABSP-5a); (E) galena with a Pb arsenate oxidation rim that has been identified as mimetite (from sample ABNWP-5a); (F) Cu–Fe arsenate particle (from sample ABNWP-1a); (G) arsenic sulfide encapsulated within silicate phases (from sample ABNWP-1a); (H) As_2O_3 particle (from sample ABNWP-1a).

in the Giant mine tailings, namely the roaster iron oxides, calcium-iron arsenate, iron oxyhydroxides, copper-iron arsenate, and lead arsenate. Data from this study show that each of the roaster iron oxide grains analyzed through EMPA contained up to 2.7 wt% antimony (Table 3). The calcium-iron arsenate and iron oxyhydroxide oxidation rims contained 0.2 wt% to 1.4 wt% antimony and 0.2 wt% to 2.1 wt% antimony respectively, while copper-iron arsenate and lead arsenate grains contained less than 0.9 wt% antimony (Table 4). EMPA data were not

Table 3
Ranges of EMPA results for Giant mine roaster Fe-oxides measured from this study and Walker (2006).

Source of Roaster Fe-Oxides	Tailings Ponds			Calcine Residue	Shoreline Tailings
Element	Fe (wt %)	As (wt %)	Sb (wt %)	As (wt%)	As (wt%)
Mean	65.5	3.0	0.8	2.9	1.3
Range	61–69	1.2–6.1	0.15–2.7	<0.5–7.6	<0.5–2.9
Std. Dev.	2.3	1.4	0.8	1.7	0.6
# grains analyzed	7			27	15
# analyses	27			63	32
Source of Data	(This study)			Walker (2006)	Walker (2006)

collected for arsenopyrite, arsenic-bearing pyrite or arsenic trioxide, but based on SEM-EDS analyses antimony was not detected in those phases. The only primary antimony phase detected in the Giant mine tailings was stibnite; however, only 1 to 16 grains of stibnite were detected in any given tailings sample.

4.1.3. XANES

Bulk XANES data show that the main oxidation states of arsenic that exist within the near-surface tailings are As^{1-} and As^{5+}, with a lesser component of As^{3+} (Fig. 3). Linear combination fitting the bulk XANES data show that samples contain 23–72% As^{1-}, 16–54% As^{5+}, and 3–31% As^{3+} (Fig. 3). Walker et al. (2015) show that roaster-derived iron oxides in the Giant mine tailings host both As^{3+} and As^{5+}; they suggest that As^{3+} is structurally incorporated into the iron oxides, while As^{5+} chemically adsorbs to the surface of the nanocrystalline minerals. Based on work by Walker et al. (2015), the arsenic contained in the roaster iron oxides at Giant mine is comprised of, on average, 39% As^{3+} and 57% As^{5+}, or an As^{3+}/As^{5+} ratio of 0.68 (±0.40). The average As^{3+}/As^{5+} ratio exhibited by the tailings samples from this study is 0.56 (±0.46).

4.1.4. μXRF and μXRD

The μXRF maps taken of the roaster-derived iron oxides show that they are predominantly comprised of iron, with a minor component of sulfur localized at the core of the phase (Fig. 6); trace arsenic is also present in the roaster iron oxides. The μXRD data show that most roaster iron oxides analyzed are maghemite, with some trace magnetite. Maghemite and magnetite exhibit similar diffraction patterns; thus, additional analyses are often required to specifically distinguish them. The maghemite and magnetite identified in the tailings samples diffracted well, exhibiting smooth Debye-Scherrer rings; this is consistent with observations by Walker et al. (2005), who propose that the nanocrystalline nature of the roaster-derived iron oxides at Giant mine result in smooth diffraction patterns.

Small particles of arsenic were observed in all μXRF maps collected for this study (Fig. 6). These particles were typically less than 20 μm in diameter, and the XRF data for these particles consistently exhibit Fe-Kα1 and Fe-Kβ1 peaks. The μXRD spectra taken of the arsenic-rich particles diffracted too poorly to match with any known phases. Comparison of the μXRF maps with SEM-BSE images suggests that these arsenic-rich particles are likely fine-grained arsenopyrite (Fig. 6), and that they may not have diffracted well due to the particles being more coarsely crystalline compared to the nanocrystalline roaster iron oxides.

The majority of the other arsenic-bearing phases identified in this study diffracted too poorly to be clearly identified via μXRD, with the exception of the lead arsenate phase. μXRF maps taken of the lead arsenate particles show that the core of these particles is generally comprised of lead and sulfur, with arsenic concentrated in surrounding oxidation rims (Fig. 7). SEM-MLA data show that the lead arsenate phase often forms an oxidation rim around galena (PbS), which comprised a minor component (i.e., less than 5%) of the sulfides in the Giant mine ore body (Jamieson, 2014). As with the roaster-derived iron oxides, the lead arsenate particles tend to diffract well and exhibit smooth Debye-Scherrer rings due to their nanocrystalline texture. The μXRD data collected for this study show that the lead arsenate particles are mimetite (Fig. 7), which is a secondary lead mineral found in circum-neutral pH environments where lead and arsenic occur together

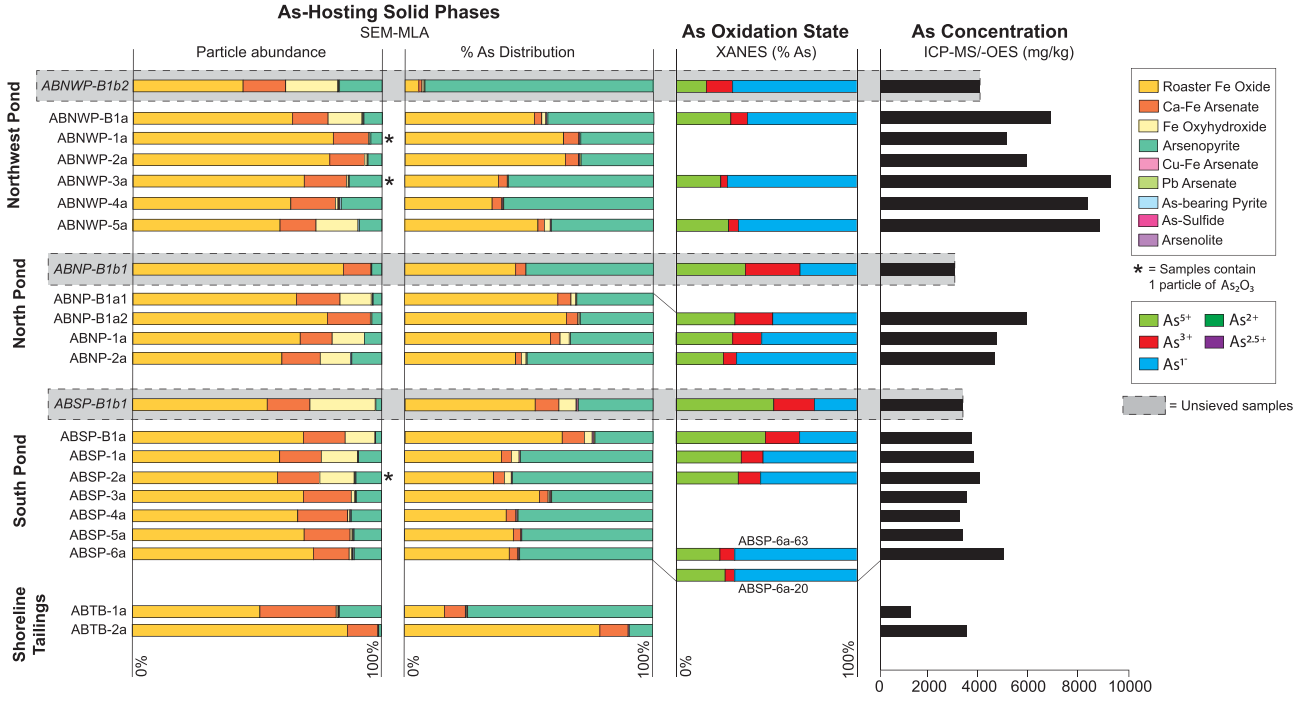

Fig. 3. Comparison of arsenic modal mineralogy results for near-surface tailings samples from SEM-MLA, As oxidation state results from XANES, and total As concentration from ICP-MS and ICP-OES. Samples highlighted in gray are unsieved samples; the other samples were sieved to <63 μm. Sample ABSP-6a-63 is of the 63-20 μm particle size fraction (from sample ABSP-6a), and sample ABSP-6a-20 is of material from the <20 μm particle size fraction (also from sample ABSP-6a).

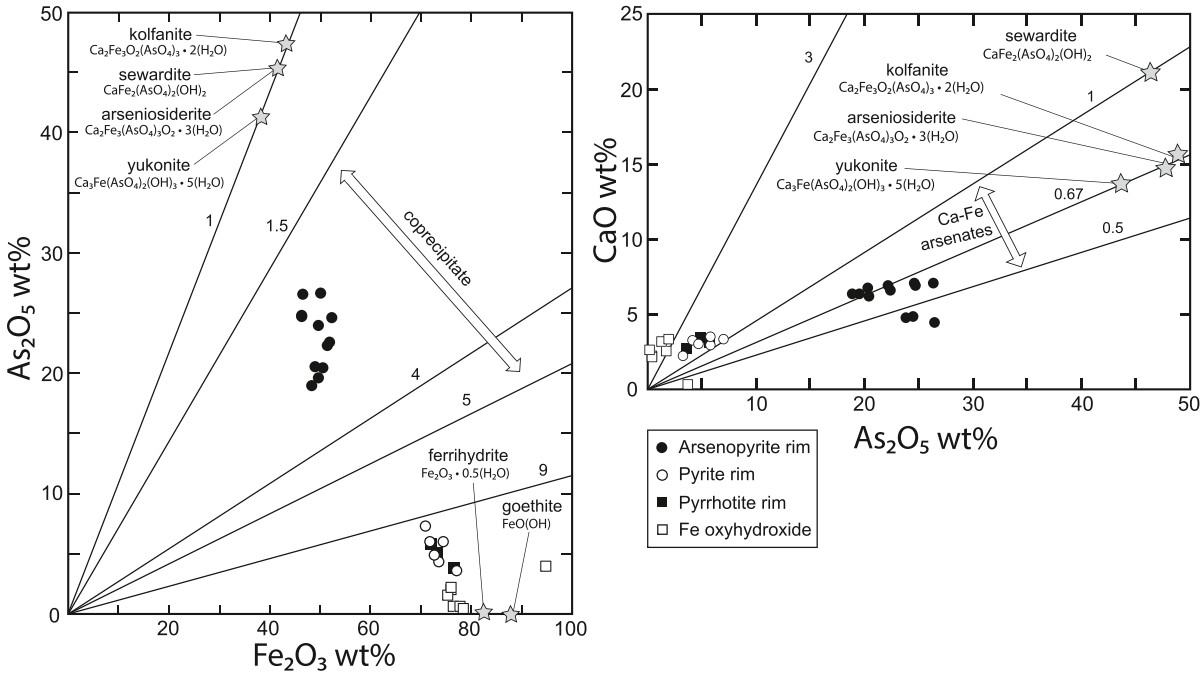

Fig. 4. EMPA data for arsenopyrite, pyrite, and pyrrhotite weathering rims and Fe oxyhydroxide particles from three of the sieved tailings samples (ABNP-1a, ABNWP-1a, ABSP-2a). On left, diagonal lines are Fe/As molar ratios; on right, diagonal lines are Ca/As molar ratios.

Table 4
Ranges of EMPA results for select elements from Cu–Fe arsenate, Pb arsenate, Ca–Fe arsenate, and Fe oxyhydroxide.

	Cu–Fe Arsenate				Pb Arsenate			Ca–Fe Arsenate				Fe Oxyhydroxide			
Element	As (wt %)	Sb (wt %)	Cu (wt %)	Fe (wt %)	As (wt %)	Sb (wt %)	Pb (wt %)	As (wt %)	Sb (wt %)	Ca (wt %)	Fe (wt %)	As (wt %)	Sb (wt %)	Ca (wt %)	Fe (wt %)
Min	2.4	0.09	7.9	5.1	3.3	0.2	44.1	12.4	0.2	3.1	32.4	0.3	0.2	0.2	49.7
Max	27.4	0.9	33.4	56.6	13.7	0.8	63.3	17.4	1.4	5.0	36.5	4.7	2.1	2.4	66.5
Mean	18.6	0.3	14.6	34.6	12.9	0.3	53.1	14.9	0.7	4.4	34.5	2.2	0.8	1.9	53.3
Std. Dev.	10.7	0.2	9.1	17.2	3.1	0.2	5.6	1.7	0.5	0.7	1.5	1.4	0.6	0.6	3.9
# grains analyzed	3				3			4				5			
# analyses	8				10			12				16			

(Bajda, 2010; Majzlan et al., 2014). This finding is supported by the EMPA results, where the bulk of the EMPA data for lead arsenate particles exhibited arsenic/lead molar ratios trending toward mimetite (Fig. 5).

4.2. TSP filter results

ICP-MS results for the TSP filters show that copper and arsenic are the most abundant metal(loid)s present in the samples, with a lesser component of antimony and lead (Fig. 8). Concentrations of these constituents remained well below the Ontario Ministry of the Environment's guidelines (Ontario Ministry of the Environment, 2012) for the duration of the sampling period, with the exception of one sample collected on June 17, 2016 where the arsenic concentration exceeded the guideline criterion of 0.3 μg/m^3 (Fig. 8). This sample was collected when the wind reached a peak velocity of approximately 6 m per second (m/s); the wind velocity was less than 5 m/s for the majority of the sampling period. The increased wind velocity most likely resulted in an increased volume of material, and thus increased load of metal(loid)s, being entrained as dust due to the greater drag force being applied to the surface material.

Two metal(loid)-bearing phases were observed in the TSP filters through SEM analysis: a copper oxide phase and an iron oxide phase (Fig. 9). The copper oxide particles vary in terms of their texture from angular and elongate to fine-grained and round; this phase was not detected in any of the near-surface tailings samples. The iron oxide particles in the TSP filters are angular and exhibit similar SEM-EDS results as the roaster-generated iron oxides that predominate the tailings in that they commonly contain arsenic. The iron oxides were the only arsenic-bearing phase that was detected in the TSP filters. Both the copper oxide and iron oxide particles were commonly observed in the <10 μm respirable fraction of the dust samples (Fig. 9).

Data for the 23 TSP filters shows that iron and arsenic exhibit a perfect positive correlation in the dust collected on site, with an R^2 value of 1.0 (Fig. 9). Iron and arsenic also exhibit near-perfect correlations with the point counting data for metal(loid)-bearing particle abundance

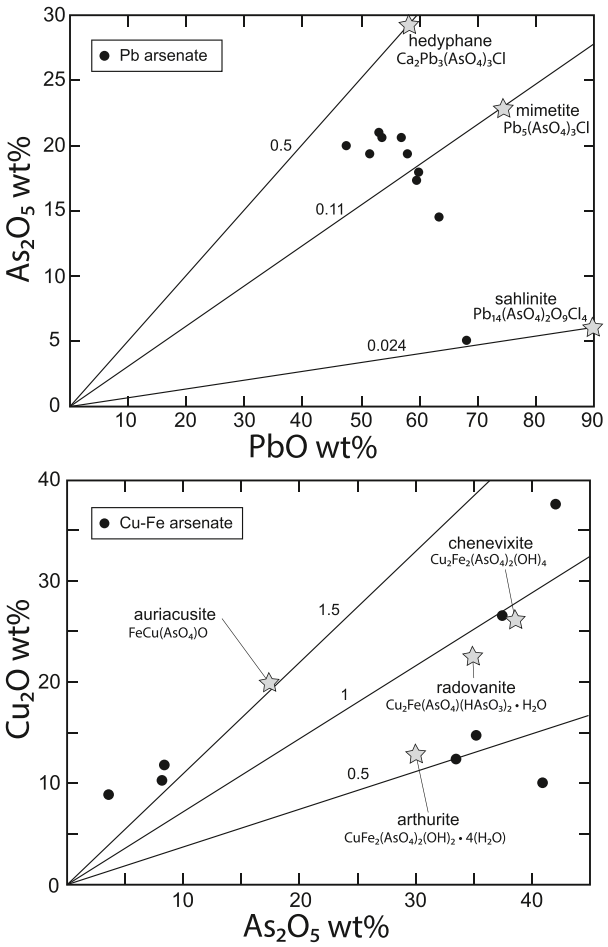

Fig. 5. On top: EMPA data for Pb arsenate grains from three of the sieved tailings samples (ABNP-1a, ABNWP-1a, ABSP-2a); diagonal lines are As/Pb molar ratios. On bottom: EMPA data for Cu–Fe arsenate grains from three of the sieved tailings samples (same as above); diagonal lines are Cu/As molar ratios.

($R^2 = 0.90$). Copper exhibits a weak correlation with the point counting data for metal(loid)-bearing particles (i.e., $R^2 = 0.12$), which suggests that it does not comprise a significant proportion of the particles in the filter samples.

5. Discussion

The results from this study show that metal(loid)s (i.e., arsenic, antimony, lead, zinc, copper, nickel) are more concentrated in the <63 μm fraction of the Giant mine tailings compared to the >63 μm fraction. This fractionation is likely due to the ore processing method that was used to produce the tailings, which involved crushing and roasting the ore to liberate the gold. The majority of the particles in the flotation tailings, produced from crushing the ore, are <75 μm in diameter, and the particles in the calcine and ESP residue, produced from roasting the ore, are mostly <45 μm and <14 μm respectively (Walker et al., 2015). Any particulate matter that is < 100 μm in diameter can be entrained by the wind, and particles between 50 and 100 μm can travel a few tens of kilometers through aeolian entrainment (Livingstone and Warren, 1996). Although only the <10 μm fraction of dust can be inhaled into the upper respiratory tract, particles greater than 10 μm in diameter can be ingested, and incidental ingestion of airborne dust can occur from dustfall coating food, drinks, and indoor/outdoor surfaces (Wiseman, 2015). Ndilo and Yellowknife are located only a few kilometers downwind of the Giant mine tailings ponds, therefore all particles found in the <63 μm fraction of the tailings pose a potential risk to local residents.

The <63 μm fraction of the tailings contain up to 9300 mgkg^{1-} arsenic, the majority of which was shown by the XANES results to be in the As^{5+} and As^{1-} oxidation states, with a lesser component of As^{3+}. Through SEM-MLA analysis, it was found that roaster-derived iron oxides, arsenopyrite, and calcium-iron arsenate host the majority of arsenic in the near-surface tailings samples. The As^{3+} that was detected in the tailings samples is attributed to the presence of roaster-derived iron oxides which have been shown by Walker et al. (2005) to host both As^{3+} and As^{5+}. In vitro extraction tests for gastric and intestinal fluids show relative arsenic bioaccessibility to be as follows: Ca–Fe arsenate = Pb arsenate = arsenic trioxide > amorphous Fe arsenate, As-bearing Fe-(oxy)hydroxides > As-rich pyrite, As sulfides (i.e., realgar) > arsenopyrite, scorodite (Meunier et al., 2010; Plumlee and Morman, 2011).

The roaster-derived iron oxides were the most abundant arsenic-hosting phase and were shown by EMPA to contain an average of 3.0 wt% arsenic. Arsenopyrite hosts 46 wt% arsenic; however, it is among the least bioaccessible arsenic hosts in gastric fluids (Meunier et al., 2010; Plumlee and Morman, 2011). Arsenopyrite grains in the near-surface tailings samples did, however, contain calcium-iron arsenate weathering rims which are highly bioaccessible according to Plumlee and Morman (2011). The iron/arsenic and calcium/arsenic molar ratio plots for the calcium-iron arsenate show that this phase is likely a co-precipitate of iron oxyhydroxide and calcium arsenate trending toward yukonite (Fig. 4). Meunier et al. (2010) found that soils from historic mine sites in Nova Scotia containing roaster-generated arsenic-bearing iron oxides (i.e., hematite and maghemite) have intermediate bioaccessibility (i.e., <5%); whereas soils containing calcium-iron arsenates are highly bioaccessible (i.e., 49%).

Two mineral phases not previously observed in the Giant mine tailings have been identified in this study: a copper-iron arsenate phase, and a lead arsenate phase. Both phases are texturally similar to the roaster-derived iron oxides in that they are porous and exhibit nanocrystalline habit (Fig. 2). The copper-iron arsenate phase exhibits significant compositional variation but diffracted too poorly to be clearly identified through μXRD analysis. The lead arsenate phase is an oxidation product of galena and was identified as mimetite through μXRD analysis (Fig. 7). This finding is supported by the arsenic/lead molar ratio plots generated for that phase from EMPA data, which show that the results are trending toward mimetite (Fig. 5). Although mimetite comprises a relatively low proportion of the <63 μm fraction of the Giant mine tailings, studies have shown fine-grained Pb arsenate can be highly bioaccessible, particularly under acidic gastric conditions (Plumlee and Morman, 2011; Ettler et al., 2019).

Based on the findings of this work, it can be concluded that arsenic trioxide is an unlikely constituent of windblown dust from the Giant mine tailings. Of the arsenic-bearing phases detected in the <63 μm fraction of the Giant mine tailings, calcium-iron arsenate and lead arsenate (i.e., mimetite) pose the greatest risk to human health as they are highly bioaccessible in gastric fluids (Plumlee and Morman, 2011; Ettler et al., 2019). Roaster-generated iron oxides (i.e., maghemite), calcium-iron arsenate, and arsenopyrite were the most abundant arsenic-bearing particles in the near-surface tailings; however, the roaster iron oxides were the only arsenic phase detected in the TSP dust samples. It is possible that the more weathered arsenic-bearing phases, such as calcium-iron arsenate and iron oxyhydroxide, are present in the dust samples but were not detected during point-counting due to their low grayscale values; however, because the multi-element data show a perfect positive correlation between arsenic and iron in the TSP filter samples (i.e., $R^2 = 1.0$), it is evident that arsenic trioxide is not present in the dust that was sampled.

Most of the tailings examined in this study were from the surface of South Pond, North Pond and Northwest Pond. The two samples from the shoreline tailings (ABTB-1a and -2a) were deposited during the early years of mine operation and uncontrolled stack emissions. It is likely that any particles of arsenic trioxide that were present in this area were

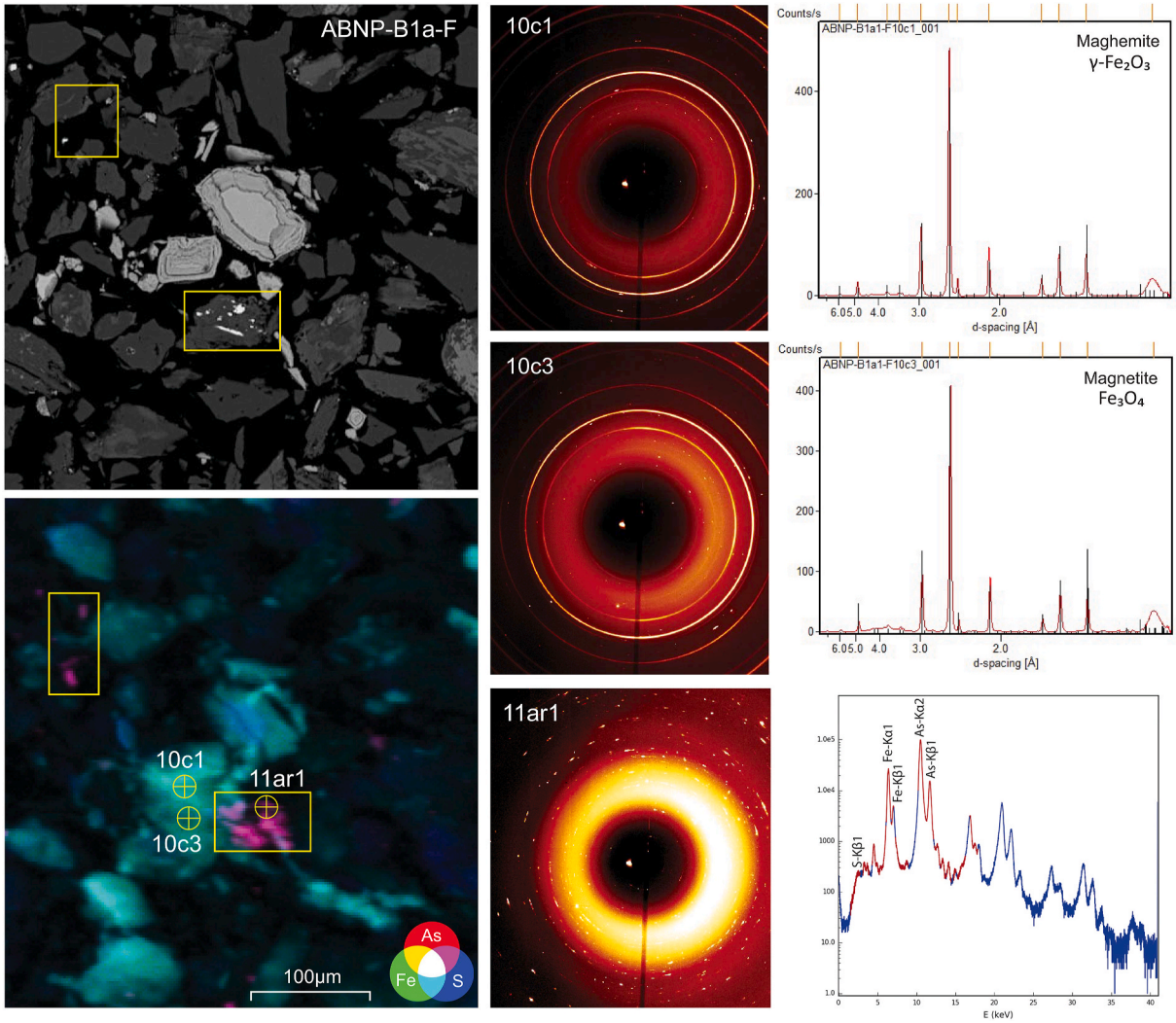

Fig. 6. Example of µXRF and µXRD data for roaster Fe-oxide and As-rich particles from sample ABNP-B1a. Peak matches for diffraction from points 10c1 and 10c3 illustrated to the right of their respective Debye-Scherrer rings; and XRF spectra for the As-rich particle (indicated by point 11ar1) illustrated in the bottom right graph. Based on the XRF results and SEM-MLA characterization, the As-rich particle at 11ar1 is identified as arsenopyrite.

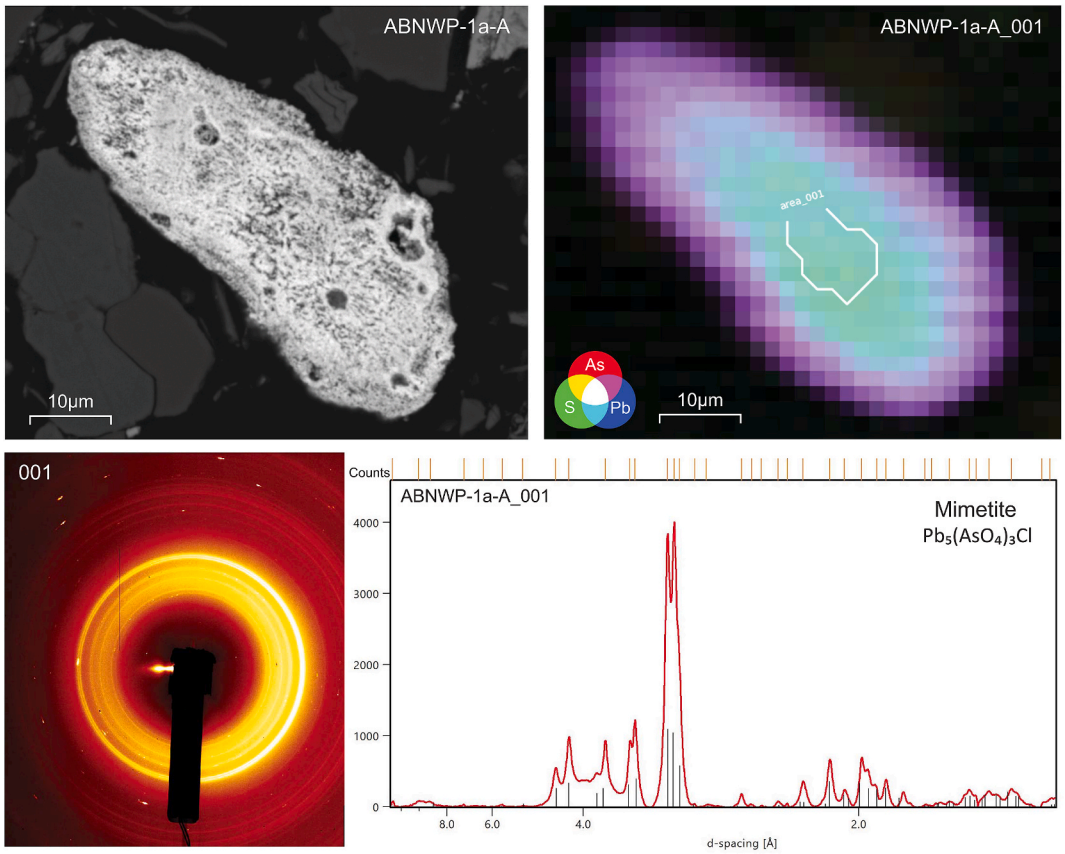

Fig. 7. µXRF and µXRD data for Pb arsenate mineral from sample ABNWP-1a, which identify the mineral as mimetite.

dissolved or physically removed by shoreline erosion processes.

The soils near the tailings ponds at Giant mine are known to contain arsenic trioxide from historic stack emissions and total arsenic concentrations similar to those of the tailings (Fig. 1; Bromstad et al., 2017). For the shallow bedrock soils on site any arsenic trioxide deposited has remained near the soil surface or exhibit slight downward migration as the arsenic trioxide dissolves (Bromstad et al., 2017; Palmer et al., 2021). However, the tailings that were exposed to roaster emissions have long since been buried by more recent tailings that do not contain arsenic trioxide. The few particles of arsenic trioxide that were observed in the tailings samples in this study may have been transported from contaminated soils adjacent to the roaster itself as windblown or vehicle-raised dust.

The fact that arsenic trioxide is able to persist in surface soils on the mine property and in the Yellowknife region suggests that if dust were to form from the soils and be transported to the community, it might actually pose a greater threat than dust formed from the tailings themselves. The dust-generating potential of the soils, which are partially vegetated, is unknown. Although the modern dust and sieved tailings characterized in this study contain almost no arsenic trioxide, surface soil samples (0–5 cm depth) taken in NDilo contain 200 to 300 $mgkg^{1-}$ arsenic, and most of this in the form of arsenic trioxide (Palmer et al., 2021). These four soil samples from Ndilo are similar in arsenic concentration and mineralogy to approximately 50 others that are within the same distance (i.e., 3 km) from the former Giant Mine (Jamieson et al., 2017; Palmer et al., 2021). The arsenic trioxide in the soil samples almost certainly represent historic deposition from stack emissions, and is not related to modern windblown dust.

6. Conclusions

Legacy mine sites such as Giant mine have lasting and complicated impacts on the surrounding environment, which makes site-wide remediation difficult to achieve. Many studies in addition to this one have found that potentially toxic metal(loid)s, including arsenic, are concentrated in the dust-sized fraction of tailings (Kim et al., 2011, 2013; Moreno et al., 2007; Martin et al., 2016; Khademi et al., 2020). The lack of arsenic trioxide in the sieved tailings collected from the Giant mine tailings ponds, which were used as proxies for modern windblown dust, is not surprising since those tailings are relatively young and would not have been impacted by the fallout of historic stack emissions from the early years of roaster operation. However, the identification of Ca–Fe arsenate as a common oxidation product of arsenopyrite suggests that windblown dust may contain fine particles of another relatively bioaccessible form of arsenic. Lead arsenate (mimetite), also not recognized previously, contains two potentially hazardous elements.

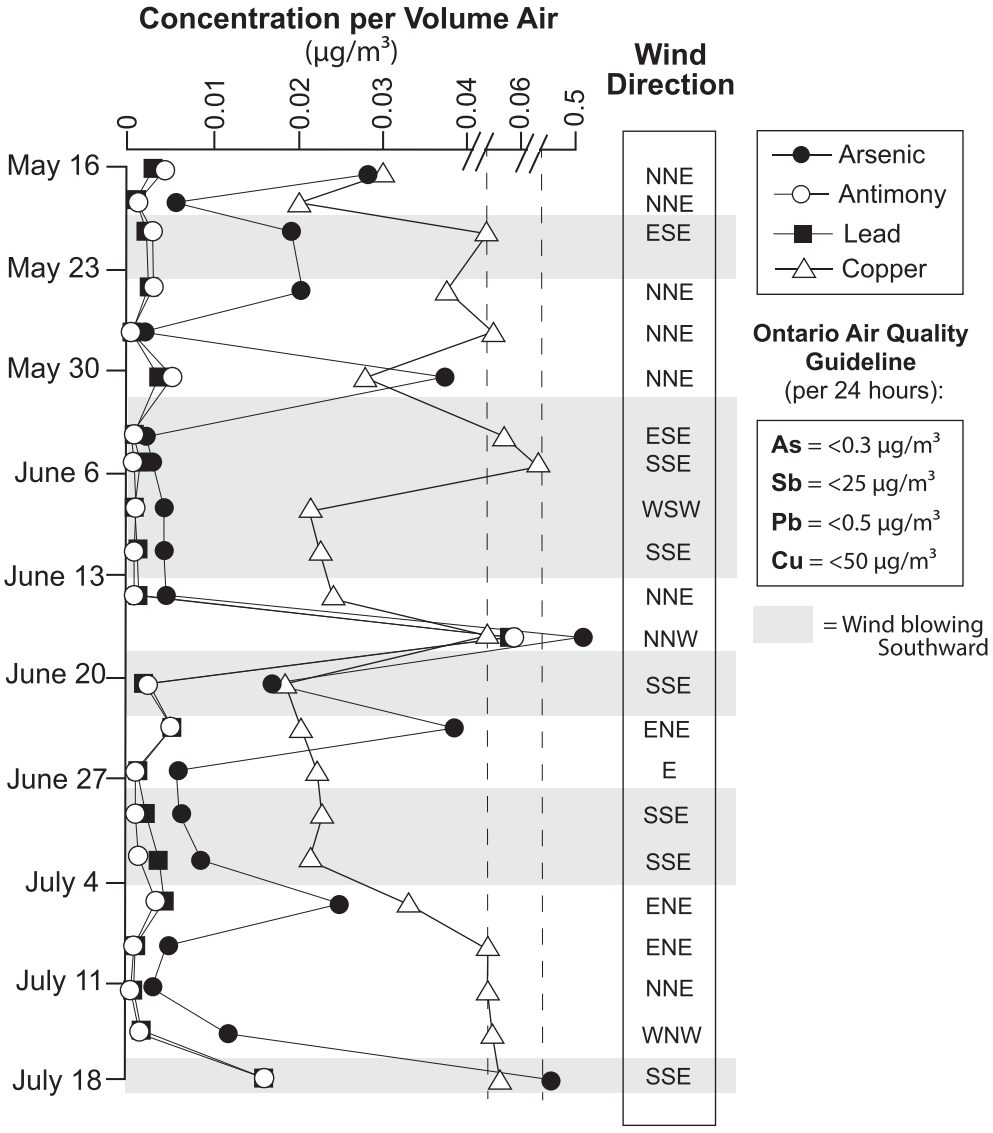

Fig. 8. ICP-MS data for As, Sb, Pb, and Cu from TSP filter samples. Data reported in ug/m3; point flow rate of sampler was 22.56 L/s. Gray boxes indicate time when wind was blowing in a Southward direction. Dashed lines indicate breaks in scale. Ontario air quality guideline values from Ontario Ministry of the Environment (2012).

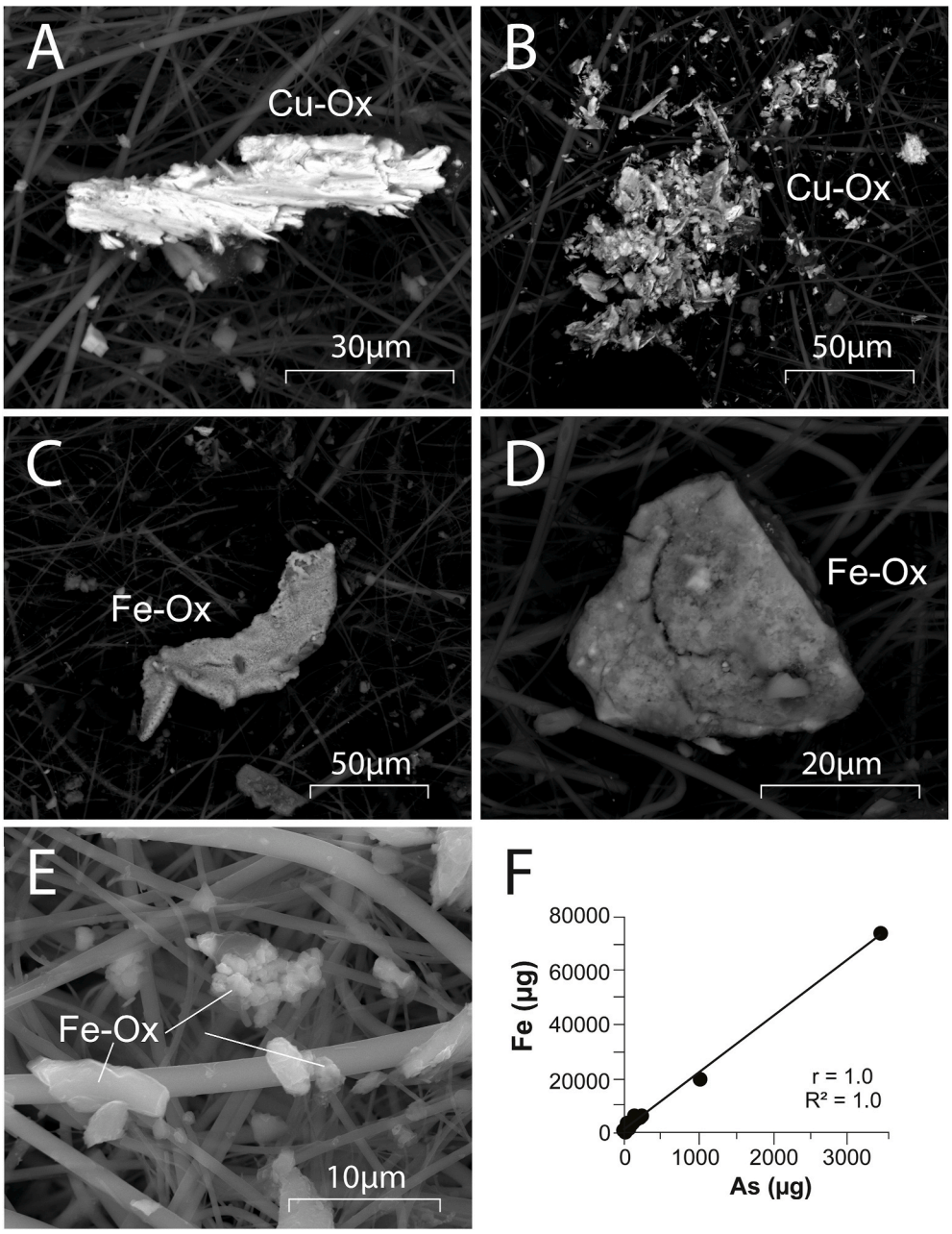

Fig. 9. (A) SEM-BSE image of an angular, elongate Cu oxide particle (from sample ABHV0514); (B) SEM-BSE image of a cluster of Cu oxide particles, both rounded and elongate (from sample AHHV0605); (C,D) SEM-BSE images of Fe-oxide particles (likely roaster-derived; C from sample AHHV0611, D from sample AHHV0608); (E) ESEM image of Fe-oxide particles in the <10 µm fraction of the dust (from sample ABHV0520); (F) regression analysis of As and Fe concentrations from all TSP filters analyzed in this study.

While the nearby community has been informed of the observation that the arsenic-bearing phases in proxy dust do not include arsenic trioxide, covering of the tailings and other measured to eliminate windblown dust will undoubtedly be welcomed.

The fact that metal(loid)s can be concentrated in the fine-fraction of mine waste highlights the importance of continuing to develop methods for understanding the solid-phase speciation of dust-sized material. Environmental contamination is not always obvious, particularly where it concerns fine-grained particulate matter. With a better understanding of contaminant speciation in dust, we can better understand and predict the ultimate fate of these contaminants in the environment and develop long-term remediation strategies at mine sites to mitigate these risks.

Funding

This work was supported by Indigenous and Northern Affairs Canada (INAC); and the Northern Scientific Training Program (NSTP).

Declaration of competing interest

The authors declare that they have no known competing financial interests or personal relationships that could have appeared to influence the work reported in this paper.

Acknowledgements

Synchrotron-based analyses were conducted at GeoSoilEnviroCARS, Sector 13-IDE, and Sector 20-BM at the Advanced Photon Source (APS), Argonne National Laboratory. Sector 13-IDE is supported by the University of Chicago, and Sector 20-BM is supported by a partnership between X-ray Science Division and the Canadian Light Source. The authors would like to thank Natalie Plato, Adrian Paradis, Tara Kramers, and all INAC staff who supported this research. Additional thanks to those at DETON'CHO/Nuna who provided on-site aid throughout sampling; J.B. Dennison and Alan Harman at SLR Consulting, Ltd., for

providing dust sampling equipment and field assistance; Agatha Dobosz and Brian Joy for their aid throughout SEM and EMP analyses; Antonio Lanzirotti who helped coordinate synchrotron analyses; and William Lines of the Yellowknives Dene First Nation (YKDFN) for keeping us informed of the community perspective.

References

Bailey, A.S., 2017. Characterization of Arsenic-Hosting Solid Phases in Giant Mine Tailings and Tailings Dust. Queen's University. MSc Thesis. https://qspace.library.queensu.ca/handle/1974/22810?show=full.

Bajda, T., 2010. Solubility of mimetite $Pb_5(AsO_4)_3Cl$ at 5-55°C. Environ. Chem. 7, 268–278.

Bromstad, M.J., Wrye, L.A., Jamieson, H.E., 2017. The characterization, mobility, and persistence of roaster-derived arsenic in soils at Giant Mine, NWT. Appl. Geochem. 82, 102–118.

CCME (Canadian Council of Ministers of the Environment), 2017. http://st-ts.ccme.ca/en/index.html.

Cleaver, A.E., Jamieson, H.E., Rickwood, C., Huntsman, P., 2021. Tailings dust characterization and impacts on surface water chemistry at an abandoned Zn-Pb-Cu-Au-Ag deposit. Appl. Geochem. 128, 104927.

Clemente, J.S., Huntsman, P., 2019. Potential climate change effects on the geochemical stability of waste and mobility of elements in receiving environments for Canadian metal mines south of 60°N. Environ. Rev. 27 (4), 478–518.

Corriveau, M.C., Jamieson, H.E., Parsons, M.B., Campbell, J.L., Lanzirotti, A., 2011. Direct characterization of airborne particles associated with arsenic-rich mine tailings: particle size, mineralogy and texture. Appl. Geochem. 26, 1639–1648.

Engelbrecht, J.P., McDonald, E.V., Gillies, J.A., Jayanty, R.K.M., Casuccio, G., Gertler, A. W., 2009. Characterizing mineral dusts and other aerosols from the Middle East – Part 1: ambient sampling. Inhalation Toxicity 21, 297–326.

Engelbrecht, J.P., Derbyshire, E., 2010. Airborne mineral dust. Elements 6, 241–246.

Ettler, V., Cihlova, M., Jarosikova, A., Mihaljevic, M., Drahota, P., Kribek, B., Vanek, A., Penizek, V., Sracek, O., Klementova, M., Engel, Z., Kamona, F., Mapani, B., 2019. Oral bioaccessibility of metal(loid)s in dust materials from mining areas of northern Namibia. Environ. Int. 124, 205–215.

Fawcett, S.E., Jamieson, H.E., 2011. The distinction between ore processing and post-depositional transformation on the speciation of arsenic and antimony in mine waste and sediment. Chem. Geol. 283, 109–118.

Hamilton, E.I., 2000. Environmental variables in a holistic evaluation of land contaminated by historic mine wastes: a study of multi-element mine wastes in West Devon, England using arsenic as an element of potential concern to human health. Sci. Total Environ. 249, 171–221.

Jamieson, H.E., 2014. The legacy of arsenic contamination from mining and processing refractory gold ore at giant mine, Yellowknife, Northwest Territories, Canada. Rev. Mineral. Geochem. 79, 533–551.

Jamieson, H.E., Maitland, K.M., Oliver, J.T., Palmer, M.J., 2017. Regional Distribution of Arsenic in Near-Surface Soils in the Yellowknife Area. Northwest Territories Open File 2017-03, 27 pages with 2 appendices.

Kastury, F., Smith, E., Lombi, E., Donnelly, M.W., Cmielewski, P.L., Parsons, D.W., Noerpel, M., Scheckel, K.G., Kingston, A.M., Myers, G.R., Paterson, D., Jonge, M.D., Juhasz, A.L., 2019. Dynamics of lead Bioavailability and speciation in indoor dust and X-ray spectroscopic investigation of the Link between ingestion and inhalation pathways. Environ. Sci. Technol. 53 (19), 11486–11495.

Khademi, H., Gabarron, M., Abbaspour, A., Martinez-Martinez, S., Faz, A., Acosta, J.A., 2020. Distribution of metal(loid)s in particle size fraction in urban soil and street dust: influence of population density. Environ. Geochem. Health 42 (12), 4341–4354.

Kim, C.S., Wilson, K.M., Rytuba, J.J., 2011. Particle-size dependence on metal(loid) distributions in mine wastes: Implications for water contamination and human exposure. Appl. Geochem. 26, 484–495.

Kim, C.S., Chi, C., Miller, S.R., Rosales, R.A., Sugihara, E.S., Akau, J., Rytuba, J.J., Webb, S.M., 2013. (Micro)spectroscopic analyses of particle size dependence on arsenic distribution and speciation in mine wastes. Environ. Sci. Technol. 47, 8164–8171.

Kříbek, B., Majer, V., Pašava, J., Kamona, F., Mapani, B., Keder, J., Ettler, V., 2014. Contamination of soils with dust fallout from the tailings at the Rosh Pinah area, Namibia: regional assessment, dust dispersion modeling and environmental consequences. J. Geochem. Explor. 144, 391–408. https://doi.org/10.1016/j.gexplo.2014.01.010.

Lippman, M., Yeates, D.B., Albert, R.E., 1980. Deposition, retention, and clearance of inhaled particles. Br. J. Ind. Med. 37, 377-362.

Livingstone, L., Warren, A., 1996. Aeolian Geomorphology: an Introduction. Longman, Harlow, pp. 1–63.

Majzlan, J., Drahota, P., Filippi, M., 2014. Parageneses and crystal chemistry of arsenic minerals. Rev. Mineral. Geochem. 79, 17–184.

Martin, R., Dowling, K., Pearce, D., Sillitoe, J., Florentine, S., 2014. Health effects associated with inhalation of airborne arsenic arising from mine operations. Geosciences 4, 128–175.

Martin, R., Dowling, K., Pearce, D.C., Florentine, S., Bennett, J.W., Stopic, A., 2016. Size-dependent characterization of historic gold mine wastes to examine human pathways of exposure to arsenic and other potentially toxic elements. Environ. Geochem. Health 38 (5), 1097–1114.

McDaniel, M.F.M., Ingall, E.D., Morton, P.L., Castorina, E., Weber, R.J., Shalley, R.U., Landing, W.M., Longo, A.F., Feng, Y., Lai, B., 2019. Relationship between atmospheric Aerosol mineral surface area and iron solubility. ACS Earth and Space Chemistry 3, 2553-2451.

Meunier, L., Walker, S.R., Wragg, J., Parsons, M.B., Koch, I., Jamieson, H.E., Reimer, K. J., 2010. Effects of soil composition and mineralogy on the bioaccessibility of arsenic from tailings and soil in gold mining districts of Nova Scotia. Environ. Sci. Technol. 44, 2667–2674.

Moreno, T., Oldroyd, A., McDonald, I., Gibbons, W., 2007. Preferential fractionation of trace metals – metalloids into PM_{10} Resuspended from contaminated gold mine tailings at Rodalquilar, Spain. Water Air Soil Pollut. 179, 93–105.

Mwaanga, P., Silondwa, M., Kasali, G., Banda, P.M., 2019. Preliminary review of mine air pollution in Zambia. Heliyon 5.

Ng, J.C., Ciminelli, V., Gasparon, M., Caldeira, C., 2019. Health risk apportionment of arsenic from multiple exposure pathways in Paracatu, a gold mining town in Brazil. Sci. Total Environ. 673, 36–43.

Ontario Ministry of the Environment, 2012. Ontario's ambient air quality criteria. http://www.airqualityontario.com/downloads/AmbientAirQualityCriteria.pdf.

Palmer, M.J., Jamieson, H.E., Borčinová Radková, A., Maitland, K.E., Oliver, J., Falck, H., Richardson, M., 2021. Mineralogical, geospatial, and statistical methods combined to estimate geochemical background of arsenic in soils for an area impacted by legacy mining pollution. Sci. Total Environ. 776, 145926.

Plumlee, G.S., Morman, S.A., Ziegler, T.L., 2006. The toxicological geochemistry of earth materials: an overview of processes and interdisciplinary methods used to understand them. Rev. Mineral. Geochem. 64, 5–57.

Plumlee, G.S., Morman, S.A., 2011. Mine wastes and human health. Elements 7, 399–404.

Pouchou, J.L., Pichoir, F., 1988. A Simplified Version of the 'PAP' Model for Matrix Corrections in EMPA. Microbeam Analysis. San Francisco Press, San Francisco, p. 315.

Querol, X., Alastuey, A., Lopez-Soler, A., Plana, F., 2000. Levels and chemistry of atmospheric particulates induced by a spill of heavy metal mining wastes in the Donana area, Southwest Spain. Atmos. Environ. 34, 239–253.

Schuh, C.E., Jamieson, H.E., Palmer, M.J., Martin, A.J., 2018. Solid-phase speciation and post- depositional mobility of arsenic in lake sediments impacted by ore roasting at legacy gold mines in the Yellowknife area, Northwest Territories, Canada. Appl. Geochem. 91, 208–220.

Sracek, O., Kříbek, B., Mihaljevič, M., Ettler, V., Vaněk, A., Penížek, V., Veselovský, F., Bagai, Z., Kapusta, J., Sulovský, P., 2021. Mobility of Mn and other trace elements in Mn-rich mine tailings and adjacent creek at Kayne, southeast Botswana. J. Geochem. Explor. 220, 106658 https://doi.org/10.1016/j.gexplo.2020.106658.

Tian, S., Liang, T., Li, K., 2019. Fine road dust contamination in a mining area presents a likely air pollution hotspot and threat to human health. Environ. Int. 128, 201–209.

Van Den Berghe, M.D., Jamieson, H.E., Palmer, M.J., 2018. Arsenic mobility and characterization in lakes impacted by gold ore roasting, Yellowknife, NWT, Canada. Environ. Pollut. 234, 630–641.

Walker, S.R., Jamieson, H.E., Lanzirotti, A., Andrade, C.F., Hall, G.E.M., 2005. The speciation of arsenic in iron oxides in mine wastes from the Giant gold mine, NWT: application of synchrotron micro- XRD and micro-XANES at the grain scale. Can. Mineral. 43, 1205–1224.

Walker, S.R., 2006. The Solid-phase Speciation of Arsenic in Roasted and Weathered Sulfides at the Giant Gold Mine, Yellowknife, NWT, Application of Synchrotron microXANES and microXRD at the Grain Scale. PhD Thesis. Queen's University.

Walker, S.R., Jamieson, H.E., Rasmussen, P.E., 2011. Application of synchrotron microprobe methods to solid-phase speciation of metals and metalloids in house dust. Environ. Sci. Technol. 45, 8233–8240.

Walker, S.R., Jamieson, H.E., Lanzirotti, A., Hall, G.E.M., Peterson, R.C., 2015. The effect of ore roasting on arsenic oxidation state and solid phase speciation in gold mine tailings. Geochem. Explor. Environ. Anal. 15, 273–291.

Webmineral, 2017. Mineralogy database. http://webmineral.com.

Wiseman, C.L.S., 2015. Analytical methods for assessing metal bioaccessibility in airborne particulate matter: a scoping review. Anal. Chim. Acta 877, 9–18.

Wrye, L.A., 2008. Distinguishing between Natural and Anthropogenic Sources of Arsenic in Soils from the Giant Mine, Northwest Territories and the North Brookfield Mine. MSc Thesis. Nova Scotia. Queen's University. https://qspace.library.queensu.ca/handle/1974/1547.